Jermy *et al. Cancer Nanotechnology* (2021) 12:33
https://doi.org/10.1186/s12645-021-00106-7

Cancer Nanotechnology

RESEARCH Open Access

Synergistic action of curcumin and cisplatin on spinel ferrite/hierarchical MCM-41 nanocomposite against MCF-7, HeLa and HCT 116 cancer cell line

B. Rabindran Jermy[1*], D. Almohazey[2], W. A. Alamoudi[3], R. M. Palanivel[4], Nora AlSudairi[5], H. Dafalla[6], A. A. Almofleh[1], T. M. Alfareed[1] and Vijaya Ravinayagam[7*]

*Correspondence:
rjermy@iau.edu.sa;
jrabindran@gmail.com;
vrnayagam@iau.edu.sa
[1] Department of Nano-Medicine Research, Institute for Research and Medical Consultations, Imam Abdulrahman Bin Faisal University, P.O. Box 1982, Dammam 31441, Saudi Arabia
[7] Deanship of Scientific Research & Department of Nano-Medicine Research, Institute for Research and Medical Consultations, Imam Abdulrahman Bin Faisal University, P.O. Box 1982, Dammam 31441, Saudi Arabia
Full list of author information is available at the end of the article

Abstract

Background: Platinum-based drugs are widely used in cancer therapy, but are known for toxic side effects and resistance. Combinational drug delivery represents an effective chemotherapeutic strategy, but often leads to an increased toxicity. Aim of this study is to test the co-delivery of cisplatin with natural antioxidants on hierarchial porous large surface area hexagonal nanocarriers for synergistic action.

Results: A series of structured mesoporous materials were impregnated with magnetic spinel ferrite (30% $CuFe_2O_4$) and then coated with curcumin (25% wt/wt). Mesosilicalite and MCM-41 with high curcumin release abilities were functionalized with cisplatin (5% wt/wt) for synergistic effect of combinational drugs. The cytotoxic efficiency of our nanocomposites was tested on cell viability of MCF7 (human breast cancer), human cervical cancer (HeLa), colorectal cancer (HCT116), and HFF (human foreskin fibroblasts) cell lines using the MTT cell viability assay. At a concentration of 0.1 mg/ml, $CuFe_2O_4$/mesosilicalite/curcumin/cisplatin resulted in 89.53% reduction in viability in MCF7, 94.03% in HeLa, 64% in HCT116 and 87% in HFF; whereas, $CuFe_2O_4$/MCM-41/curcumin/cisplatin resulted in 76% reduction in viability in MCF7, 64.46% in HeLa, 64% in HCT116 and 24% in HFF. The EC_{50} for $CuFe_2O_4$/mesosilicalite/curcumin/cisplatin was 81.23 µg/ml in MCF7, 47.55 µg/ml in HeLa, 48.96 µg/ml in HCT116 and 76.83 µg/ml in HFF. The EC_{50} for $CuFe_2O_4$/MCM-41/curcumin/cisplatin was 72.51 µg/ml in MCF7, 58.6 µg/ml in HeLa, 62.58 µg/ml in HCT116 and 154.2 µg/ml in HFF. Furthermore, cells treated with both nanocomposites had a high number of cleaved Caspase 3-positive cells suggesting that the reduction in cell viability was triggered by activating the apoptotic signaling pathway.

Conclusion: Our results show that $CuFe_2O_4$/MCM-41/curcumin/cisplatin is a better candidate for combinational drug therapy due to its lowest EC_{50} value and the wider difference in EC_{50} (a fold change) between cancerous and non-cancerous cell line.

Keywords: Multifunctional, Curcumin, Coating, cisplatin, MCM-41, Nanotherapeutics

Introduction

In recent years, magnetic nanoparticles in nanomedicine research have been steadily rising for developing targeted drug delivery system for various biomedical applications (Amiri et al. 2019). Spinel ferrite-based nanocomposites have been widely studied in biomedical applications such as hyperthermia, contrasting agents in tumor imaging, drug delivery and magnetic separation of biological specimens (Kefeni and Mamba 2020). The use of magnetic nanocomposites in drug delivery has been reported to increase the targeted drug delivery, reduce the dose, and enhance patient compliance (Ghosh et al. 2019). Among the different types of spinel ferrites, $CuFe_2O_4$ is an interesting magnetic nanoparticle due to its superparamagnetic nature, strong T2 MRI contrast, ability to be guided by an external magnetic field, tunable particle size, low synthesis cost, and its eco-friendly characteristics (Khanna et al. 2019). $CuFe_2O_4$ was composed of a cubic inverse spinel structure in the Fd3m space group (Dippong et al. 2021). Several nanocarriers with functionalization property based on hydrogels, alginate, clay, liposomes and polymeric species based therapeutic tools have been reported for treating chronic diseases (Li et al. 2019; Mantha et al. 2019; Abduljauwad and Ahmed 2019; de Lima et al. 2018). Mesoporous hexagonal structured silica MCM-41 with superior textural features with high surface area (~500–1000 m^2/g) has been used as catalyst in fine chemical synthesis and gas adsorption (Beck et al. 1992; Lanzafame et al. 2020; Chen et al. 2020). The large hexagonal shaped pore size of Si-MCM-41 is built with amorphous silica framework. ZSM-5/MCM-41 hybrid composite material that are derived from zeolite contains crystalline framework with presence of micropore and mesopores (Ravinayagam and Jermy 2019; Odedairo et al. 2012). The framework of such hierarchical hexagonal structure of composite is stable due to nanozeolitic building units (Jermy and Ravinayagam 2019).

Recently, using multiple drug-loaded nanoparticles had attracted interest as a cancer treatment option to overcome drug resistance. Xylan, a polysaccharide biopolymer modified with a redox-sensitive conjugate disulfide linker, has been explored as a drug delivery system. The delivery of curcumin and 5-fluorouracil using xylan nanoparticles resulted in a significant inhibition of cell viability in the colon carcinoma cells HT-29 and HCT-15 (Sauraj et al. 2020). Biocompatible polymers involving polyethylene glycol and poly(lactic-co-glycolic acid) exhibited a superior release of antineoplastic drug (7-ethyl-10-hydroxycamptothecin) and curcumin. The nanocomposite formulation with hydrophobic coating (dioleoylphosphatidic acid) has shown significant reduction in cell viability of cervical and ovarian cell lines (HeLa, A2780) (Li and Gao 2020). Layer-by-layer deposition of natural polysaccharide chitosan and negatively charged dextran sulfate has been reported using double-emulsion cross-linking technique. Chitosan–paclitaxel was prepared using internal oil in water emulsion. After addition of external water to oil emulsion, dextran sodium and chitosan bound 5-fluorouracil were added and then lyophilized. The dual drug-loaded nanoparticles with particle diameter of about 292 nm were reported to induce significant reduction in cell viability of HepG2 cells (Wang et al. 2020). A bilayer structured vesicle Niosome functionalized with folic acid was found to be effective as a dual drug carrier of curcumin and letrozole. Non-ionic surfactant Span 80 and cholesterol (lipid) to drug ratio optimization resulted in high drug encapsulation. The synergism between both drugs was observed to inhibit the

viability of breast cancer cells (MCF-7 and MD-MB-231) leading to downregulation of Bcl2, cyclin D and cyclin E genes and upregulation of p53, Bax, caspase-3 and caspase-9 genes (Akbarzadeh et al. 2020). We have synthesized several zeolites and expanded their applications from traditional petrochemical applications to biomedical applications including drug delivery and diagnostic applications (Jermy et al. 2019; Jermy and Ravinayagam 2019). Curcumin is less-soluble antioxidant and therefore has lower bioavailability that prevents the advantages of curcumin for therapeutics (Karthikeyan et al. 2020). The presence of curcumin along with Pt compound over mesoporous drug delivery system has multiple advantages. The encapsulation of curcumin inside the nanopores is expected to improve the solubility, bioavailability and target specificity. The presence of cisplatin can influence a synergistic effect with curcumin and spinel is expected to be beneficial for imaging. Till now, the combinational effect of curcumin and cisplatin was not explored on spinel-based hierarchical micro/mesoporous materials like mesosilicalite and mesoporous MCM-41.

In the present study, the effect of copper spinel impregnation into mesosilicalite and MCM-41 was explored for dual release of curcumin and cisplatin. The study shows that spinel, curcumin and cisplatin loading varies with pore structures of mesosilicalite and MCM-41. Micro- and meso-pores containing mesosilicalite is more potent as a cytotoxic agent in both cell lines. However, mesoporous MCM-41 is a better candidate due to the wider difference in cytotoxic capability in cancerous and non-cancerous cell lines.

Material and methods

Ludox AS-40 (silica source), tetrapropylammonium bromide (micropore template), cetyltrimethyl ammonium bromide (mesoporous template), copper nitrate, iron nitrate, and anticancer drug (cisplatin) were purchased from Sigma Aldrich. Curcumin was obtained from Molecule on (New Zealand). Q-10 silica with pore diameter of about 18 nm was obtained from Fuji Silysia Chemical Ltd, Japan. Spherical hydrophobic silica was purchased from Superior Silica, USA. All the reagents used in in vitro study were of analytical grade. Cell culture reagents: DMEM (Dulbecco's modified Eagle medium), heat-inactivated fetal bovine serum (HI-FBS), 100X penicillin streptomycin, and 100X MEM NEAA (MEM non-essential amino acids) were obtained from Gibco, Thermo Fisher Scientific. 3-(4,5-dimethylthiazol-2-yl)-2,5-diphenyltetrazolium bromide (MTT) reagent, cat. M2128 was purchased from Sigma-Aldrich. Hoechst 33342 nuclear stain, cat. 62249, and cleaved-Caspase antibody 3 (c-Caspase 3), cat. 9661, were procured from Thermo Fisher Scientific and Cell Signaling Technology, respectively. Alexa Fluor 594 goat anti-rabbit secondary antibody, cat. R37117 was obtained from Invitrogen, Thermo Fisher Scientific.

Preparation of 30%$CuFe_2O_4$/mesosilicalite and 30%CuFe2O4/MCM-41

Mesosilicalite was prepared by disintegrating silicalite crystals in alkaline medium following the top-down approach. A detailed synthesis procedure for mesosilicalite, MCM-41, SBA-16, and mesobeta are provided in our previous publication (Ravinayagam and Jermy 2017). The copper ferrite-impregnated mesosilicalite and MCM-41 were prepared by dry mixing. Briefly, 0.61 g of copper nitrate trihydrate, 1.01 g of iron nitrate

nonahydrate and 1.4 g of predried structured silica were physically mixed for 30 min using mortar pistol. The obtained mixture was calcined at 850 ℃ for 6 h.

Curcumin loading over 30%$CuFe_2O_4$/structured silicas

In the first step, curcumin was loaded on a series of copper spinel-loaded structured silicas. 40 mg of curcumin was dissolved in 10 ml of methanol for 10 min. Then 160 mg of respective spinel-loaded structured silicas (mesosilicalite, MCM-41, SBA-16, Q10 silica, hydrophobic silica, mesobeta, mesoZSM-5) was added and the mixture was sonicated for 2 min. Then the solvent was evaporated using rotary evaporator.

For selected sample like $CuFe_2O_4$/mesosilicalite/curcumin and $CuFe_2O_4$/MCM-41/curcumin, cisplatin was loaded. In this step, cisplatin (30 mg) was first added in normal saline solution.

(10 ml) and stirred to form a clear solution. Then, $CuFe_2O_4$/mesosilicalite/curcumin or $CuFe_2O_4$/MCM-41/curcumin (600 mg) was added and stirred overnight under ice cold dark environment. The solution was then filtered, washed and dried. The functionalized cisplatin was estimated using UV–visible spectroscopy at 208 nm.

Characterization techniques

The phase of spinel-loaded support carriers $CuFe_2O_4$/mesosilicalite, $CuFe_2O_4$/MCM-41, $CuFe_2O_4$/SBA-16, $CuFe_2O_4$/hydrophobic silica, $CuFe_2O_4$/MesoZSM-5 and $CuFe_2O_4$/mesobeta was identified using benchtop XRD (Miniflex 600, Rigaku, Japan). The textural features including BET surface area, pore size and pore volume were measured using nitrogen adsorption technique (ASAP-2020 plus, Micromeritics, USA). The ferrite nanoparticle chemical coordination was analyzed using DRS-UV–visible spectroscopy analysis (JASCO, Japan). Vibrating sample magnetometer (LDJ electronics, 9600) was used to determine the magnetic property of $CuFe_2O_4$/mesosilicalite and $CuFe_2O_4$/MCM-41. The functional groups of curcumin and cisplatin in our nanoformulation were determined using FT-IR spectroscopy (Perkin Elmer). The morphological variations of spinel ferrite/mesosilicalite/curcumin/cisplatin were investigated using transmission electron microscopy (TEM, JEM2100F, JEOL).

Curcumin release study

In the first step, curcumin release was studied over different copper spinel-loaded structured silicas. The release study was carried out by dissolving 30 mg of curcumin-loaded sample in 50 ml of PBS (pH 5.6). The curcumin release was monitored at 37 °C. At regular time interval, 10 ml of solution was withdrawn and replaced with equal volume of fresh solution. The curcumin release content was identified at specific wavelength of 428 nm. $CuFe_2O_4$/mesosilicalite/curcumin/cisplatin and $CuFe_2O_4$/MCM-41/curcumin/cisplatin were chosen for cisplatin release. The cisplatin release was measured at 208 nm using UV–visible spectroscopy.

Cell culture

We used human mammary adenocarcinoma (MCF7)), human cervical cancer (HeLa), colorectal cancer (HCT116), and the non-cancerous human foreskin fibroblasts (HFF) cell lines to assess the cytotoxic effect of our compounds. Cells were cultured in a DMEM culture

medium containing 10% HI-FBS, 1% penicillin streptomycin, and 1% MEM NEAA. Cells were maintained in a humified setting at 37 °C with 5% CO_2. For cell viability assay, cells were seeded in a 96-well plate with a density of 20,000 cells/well. For immunofluorescent staining, 50,000 cells/well were plated on eight-well chamber slides. On the following day, cells were switched to the starve culture medium that contains 0.5% HI-FBS. On the next day, cells were treated with our nanocomposites as described in the following section.

Cell treatment

MCF7 and HFF cells were treated with the subsequent conditions for 48 h: $CuFe_2O_4$/mesosilicalite, curcumin, cisplatin, curcumin/cisplatin, $CuFe_2O_4$/mesosilicalite/curcumin, $CuFe_2O_4$/mesosilicalite/curcumin/cisplatin and $CuFe_2O_4$/MCM-41/curcumin/cisplatin. Treatment concentrations of $CuFe_2O_4$/mesosilicalite, $CuFe_2O_4$/mesosilicalite/curcumin, $CuFe_2O_4$/mesosilicalite/curcumin/cisplatin, and $CuFe_2O_4$/MCM-41/curcumin/cisplatin nanocomposites were: 0.025, 0.05, 0.1, and 0.5 mg/ml. Based on the drug-loading experiments, simple calculations were followed to reflect the actual quantity of curcumin and cisplatin that was adsorbed on $CuFe_2O_4$/mesosilicalite and $CuFe_2O_4$/MCM-41 nanoparticles. According to the loading experiments, 1 mg of $CuFe_2O_4$ nanoparticles contains 0.25 mg and 0.045 mg of curcumin and cisplatin, respectively. Thus, if $CuFe_2O_4$/mesosilicalite concentration was 0.5 mg/ml, there is 0.125 mg/ml of adsorbed curcumin and 0.0225 mg/ml of functionalized cisplatin. Therefore, the treatment concentrations of curcumin were: 0.00625, 0.0125, 0.025 and 0.125 mg/ml and the treatment concentrations of cisplatin were: 0.001125, 0.00225, 0.0045 and 0.0225 mg/ml.

Cell viability (MTT) and EC50

To assess the cytotoxicity of our compounds, we used 3-(4,5-dimethylthiazol-2-yl)-2,5-diphenyltetrazolium bromide (MTT), a cell viability assay. It measures the cell viability by assessing the ability of mitochondria to convert yellow MTT solution into purple formazan insoluble crystals. Following Mosmann (1983) protocol, 5 mg/ml of MTT powder was dissolved in PBS, and 0.5 mg/ml of MTT working solution was prepared. Cells were washed with PBS and followed by the addition of 100 µl MTT working solution. All the experimental conditions were run in triplicates (technical repeats) with five biological repeats (n=5). The 96-well plate was incubated for 3 h at 37 °C. An MTT negative control (background control) was included in the experimental setting by adding MTT working solution to wells that contain no cells. After the incubation time, 0.04 N HCl isopropyl alcohol was added to solubilize the formazan crystals. The difference in color intensity was measured by SYNERGY-neo2 BioTek ELISA reader at 570 nm. The technical triplicate readings of each condition were averaged, and the absorbance from MTT negative control was deducted from these readings. An initial reading was measured before MTT addition to exclude background interference. The initial reading was subtracted from the final reading. Then, the treatment groups were analyzed by comparing them to the control (untreated cells). Cell viability was calculated using the following equation:

$$\%\ \text{Cell viability} = \times 100.$$

Data from the cell viability assay were used to calculate the half-maximal effective concentration (EC_{50}) using Prism 9 software (GraphPad, La Jolla, CA). Concentration values

were transformed to logarithmic data. Then, a sigmoidal curve was selected to fit the data and generate the calculated log EC_{50}, EC_{50}, and R^2 values for each condition.

Immunofluorescent staining

As mentioned above, cells were plated in an 8-well chamber slide at a concentration of 50,000 cells/well. Cells were then treated for 48 h with the following conditions: $CuFe_2O_4$/mesosilicalite/curcumin, $CuFe_2O_4$/mesosilicalite/curcumin/cisplatin, and $CuFe_2O_4$/MCM-41/curcumin/cisplatin at a concentration of 0.5 mg/ml. Cells were fixed and stained with the apoptotic marker cleaved Caspase 3 (c-Caspase 3) antibody (1:200, Cell Signaling Technology) and incubated at 4 °C overnight. After PBS washing, Alexa Fluor 594-conjugated secondary antibody (Invitrogen, Thermo Fisher Scientific) was added to the cells at a final concentration of 1:1000 for 1 h at room temperature. Cells were then washed and stained with the nuclear stain Hoechst 33,342 (Thermo Fisher Scientific) at a concentration of 2 μg/ml and incubated at room temperature for 20 min. After staining, immunofluorescent images were taken using a confocal fluorescent microscope—Zeiss LSM 700. Bright-field images were captured using an inverted microscope—Nikon Eclipse TS100. Although both light and fluorescent pictures were taken from the same sample, they were not taken from the same field of view.

Statistics

The cell viability assay was performed in five independent experiments (n=5). Statistical analysis was performed using Prism 9 software (GraphPad, La Jolla, CA). The analysis was performed using one-way ANOVA with Dunnett's post hoc test. Error bars ± S.E.M. * $p<0.05$; ** $p<0.01$; *** $p<0.001$; **** $p<0.0001$ versus control. In case there was no indication of significance, it means that results were non-significant. The data analysis of drug delivery was done using Prism 8 software and SPSS software version 20.0.

Results and discussion

The X-ray diffraction patterns of meso- and micro-phases of two supports were identified at low and high angle of MCM-41 and mesosilicalite (Fig. 1). The XRD pattern of $CuFe_2O_4$ impregnated over different structured nanocarriers is shown in Additional file 1: Fig. S1. Conventional MCM-41 showed a typical hexagonal peaks at low angle corresponding to the plane (100), (110) and (200). Mesosilicalite showed the presence of MCM-41 and high silica zeolite peaks at 2 theta value of 7.9° and 8.7° corresponding to plane (101) and (200), respectively. In the higher angle (20–60°), a broad peak of MCM-41 indicates the presence of amorphous framework bound to hexagonal phase. Mesosilicalite showed the typical characteristics peaks of MFI structure with corresponding to (321), (113), (501), (422) and (313) plane. In case of spinel impregnated MCM-41 and mesosilicalite, the presence of cubic phase of copper spinel appears with intense peak at 35.6° corresponding to (103) plane. A trace of α-Fe_2O_3 appears along with a less intense peak corresponding to CuO at 38.7°.

The characteristics of textural surface, pore volume and average pore size of (a) MCM-41, (b) CuFe2O4/MCM-41, (c) mesosilicalite and (d) CuFe2O4/mesosilicalite are shown in Fig. 2. The surface area and pore size distribution of $CuFe_2O_4$ impregnated over different structured materials are shown in Additional file 1: Figs. S2 and

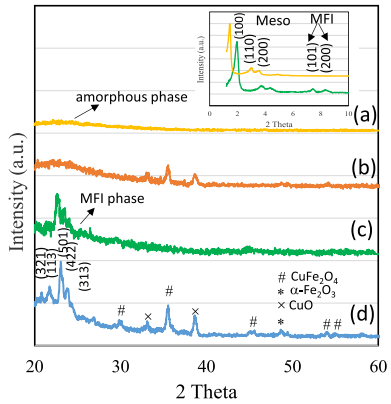

Fig. 1 X-ray diffraction pattern of **a** MCM-41, **b** $CuFe_2O_4$/MCM-41, **c** mesosilicalite and **d** $CuFe_2O_4$/mesosilicalite

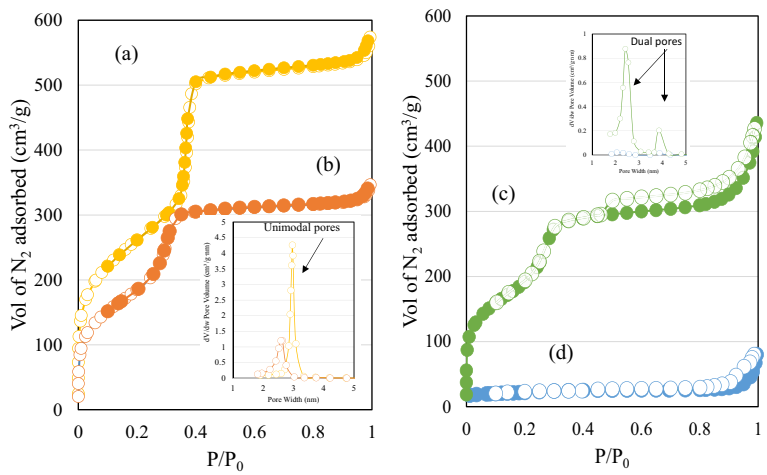

Fig. 2 Nitrogen adsorption isotherm pattern of **a** MCM-41, **b** $CuFe_2O_4$/MCM-41, **c** mesosilicalite and **d** $CuFe_2O_4$/mesosilicalite

S3. Before, spinel ferrite impregnation, MCM-41 showed a typical type IV isotherm indicating the presence of uniform pore size distributions (3.7 nm) with high surface area of 914 m^2/g and pore volume of 0.85 cc/g (Additional file 1: Table S1). In case of pure hexagonal mesopores of MCM-41, surprisingly, impregnation of spinel, only slightly reduced the surface area to 885 m^2/g, while pore volume reduced to 0.52 cc/g. In case of mesosilicalite, which contains micro- and mesopores, the initial surface area of 804 m^2/g reduced significantly after impregnation to 74 m^2/g. An increase in dual pore sizes from 3.0 nm to 5.9 nm indicates the pore-filling effect and formation of external pores in the hierarchical micro- and meso-pores after spinel ferrite loading. Pore volume reduction from 0.6 cc/g to 0.1 cc/g reflects the pore-filling effect. Overall, the result shows unique deposition of spinel occurs over two supports. The textural characteristics vary depending on the structure of different shaped materials (Additional file 1: Table S1).

The rearrangement of curcumin and cisplatin over $CuFe_2O_4$/mesosilicalite was analyzed using TEM, FTIR and diffuse reflectance spectra analysis (Fig. 3A–F). The morphological feature of mesosilicalite/Pt without curcumin coating and after coating sample $CuFe_2O_4$/mesosilicalite/curcumin/cisplatin was analyzed using transmission electron microscope at different scale bar of 100 nm, 50 nm and 10 nm (Fig. 3A–D). In case of mesosilicalite/Pt sample, the presence of micro- and meso-phase is clearly seen. The presence of discontinuity as white dots indicates the nanozeolitic microphase, while continued pore channels shows the hexagonal mesopore ordering (Fig. 3A). After curcumin coating, the images shows the presence of curcumin at the external surface of MCM-41 (Fig. 3B and C). Further magnification to 10 nm, a uniformly layered hexagonal pore channels can be clearly seen to coexist with curcumin (Fig. 3D). The FT-IR spectra of cisplatin, curcumin, $CuFe_2O_4$/mesosilicalite, $CuFe_2O_4$/mesosilicalite/curcumin and $CuFe_2O_4$/mesosilicalite/curcumin/cisplatin are shown in Fig. 3E(a-e). Drug cisplatin showed a characteristic functional group related to NH group of platinum complex between 400 and 1800 cm^{-1}. A symmetric and asymmetric bending of NH_2 group was

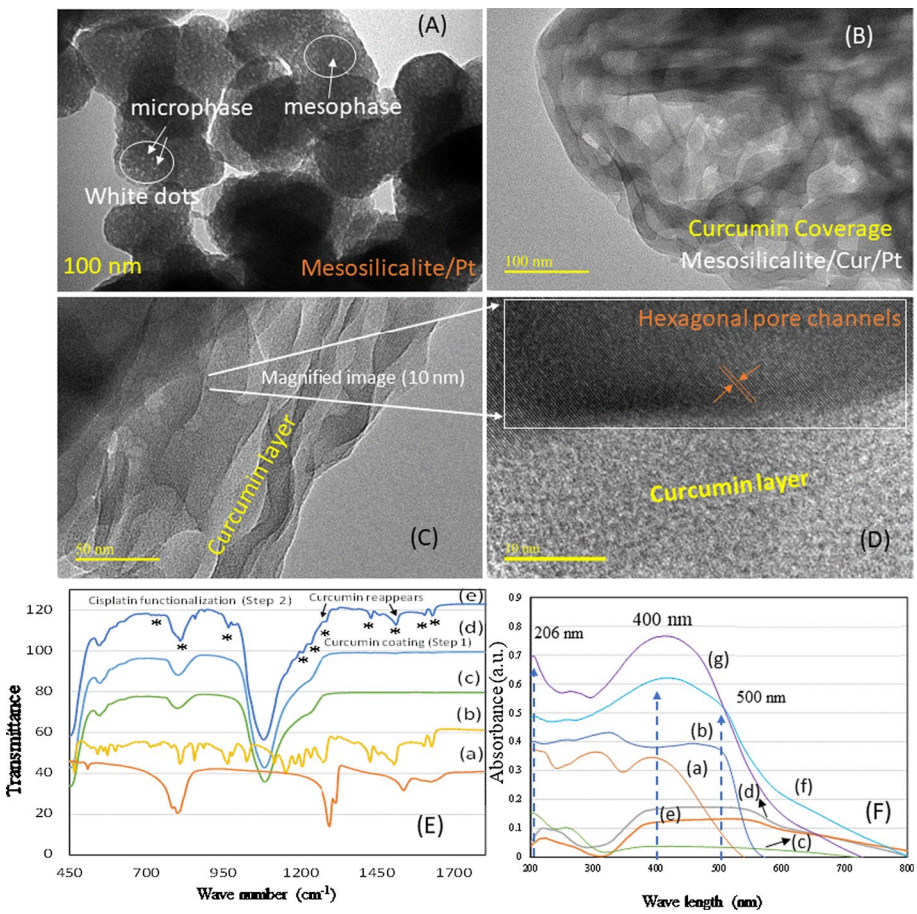

Fig. 3 **A**–**D** Transmission electron microscope of mesosilicalite/Pt, $CuFe_2O_4$/mesosilicalite/curcumin/cisplatin at different scale bar of 100 nm, 50 nm and 10 nm. Figure 3E. FTIR spectra of **a** cisplatin, **b** curcumin, **c** $CuFe_2O_4$/mesosilicalite, **d** $CuFe_2O_4$/mesosilicalite/curcumin and **e** $CuFe_2O_4$/mesosilicalite/curcumin/cisplatin. **F** Diffuse reflectance UV–visible spectra of **a** cisplatin, **b** curcumin, **c** MCM-41, **d** $CuFe_2O_4$/mesosilicalite, **e** $CuFe_2O_4$/MCM-41, **f** $CuFe_2O_4$/mesosilicalite/Cur/Pt and **g** $CuFe_2O_4$/MCM-41/Cur/Pt

clearly observed between 1300 and 1600 cm^{-1}, while plane bending of cisplatin can be seen at about 800 cm^{-1} (Fig. 3Ea). In case of curcumin, the presence of carbonyl (C=O), carbon–carbon double bond (C=C), and methylene (CH_2) bending peaks are observed between 1625 and 1450 cm^{-1}. Both symmetric and asymmetric vibrations corresponding to ether bond (C–O–C) are observed between 1300 and 1000 cm-1 (Bhandari et al. 2016) (Fig. 3Eb). A peak corresponding to enolic OH group of curcumin appears clearly at about 960 cm^{-1}. In case of $CuFe_2O_4$/mesosilicalite, a zeolitic peak indicating hybrid formation between mesoporous and microporous zeolite appears at about 550 cm^{-1} (Fig. 3Ec). After curcumin coating (curcumin loading step 1), the sample $CuFe_2O_4$/mesosilicalite/curcumin showed no distinct peaks of curcumin. However, a significant reduction in hydroxyl group of enol indicates an effective interaction inside the mesosilicalite pores and curcumin (Fig. 3Ed). Unexpectedly, the $CuFe_2O_4$/mesosilicalite/curcumin/cisplatin (cisplatin loading step 2) sample, the loading of cisplatin showed the peaks of curcumin. It indicates that during cisplatin functionalization step, curcumin present inside the pores of mesosilicalite diffuses out and present at the external surface of mesosilicalite (Fig. 3Ee). In addition, a peak at about 1023 cm^{-1} indicates the C–O–C stretching of C_6H_5–O–CH_3 group (Mohan et al. 2012). Also, the presence of cisplatin peaks reveals an effective functionalization of drug at external surface of mesosilicalite. Figure 3Fa–g shows the diffuse reflectance UV–visible spectra of curcumin, cisplatin, MCM-41, $CuFe_2O_4$/MCM-41, $CuFe_2O_4$/mesosilicalite, $CuFe_2O_4$/MCM-41/curcumin/cisplatin and $CuFe_2O_4$/mesosilicalite/curcumin/cisplatin. Curcumin and cisplatin revealed broad absorption between 200 and 600 nm (Fig. 3Fa and b). The support SiMCM-41 showed the absorption bands at about 210 and 260 nm, indicating the framework coordinated siliceous species (Fig. 3Fc). In case of $CuFe_2O_4$/MCM-41 and $CuFe_2O_4$/mesosilicalite, the spectra showed a weak absorption below 230 nm and a strong and broad absorption between 240 and 800 nm (Fig. 3Fd and e). The peaks of $CuFe_2O_4$/MCM-41 and $CuFe_2O_4$/mesosilicalite correlate with cubic spinel exhibits tetrahedral (215 nm) and octahedral (440–700 nm) crystalline coordination sites (Najmoddin et al. 2014). The presence of such peak absorption indicates the dispersion and integrated spinel ferrites over both supports. Importantly, in case of mesosilicalite support, an enhanced intense broad peak shows the presence of higher crystalline mixed phase of oxides due to octahedral coordinated spinel species compared to the MCM-41 support. This can be attributed mainly due to presence of micropores, which tends to accommodate spinel species at the external surface of mesosilicalite. After loading of curcumin and cisplatin, the absorption maximum increases significantly over both $CuFe_2O_4$/mesosilicalite and $CuFe_2O_4$/MCM-41 nanocomposites. However, in case with $CuFe_2O_4$/mesosilicalite/curcumin, a two distinct band absorptions at about 400 nm and 500 nm clearly indicates the distributed curcumin and Pt species (Fig. 3Ff). However, with $CuFe_2O_4$/MCM-41/curcumin, a broadness of absorption peak indicates cohabitation of curcumin and Pt species over MCM-41 (Fig. 3Fg). Such increase in homogenous expansion behavior clearly indicates the composite formation over mesoporous MCM-41 support than with mesosilicalite. As detected in XRD and DRS-UV analysis (Figs. 1 and 3F), though the active spinel metal components were not observed in TEM analysis, the migration of curcumin can be clearly observed as a surface coating at the external surface of mesosilicalite.

The magnetic characteristics and saturation value of $CuFe_2O_4$/MCM-41 and CuFe2O4/mesosilicalite nanocomposites were analyzed by vibrating sample magnetometer at room temperature (Additional file 1: Fig. S4a and b). A distribution of cations at different coordination sites of A and B characterize the magnetic property. $CuFe_2O_4$/MCM-41 and $CuFe_2O_4$/Mesosilicalite showed ferromagnetic property with saturation magnetization value of about 0.9 emu/g. The saturation magnetization value was reported to be related to the magnetic phase concentration. Fe loaded on high surface area MCM-41 was reported to exhibit magnetization of 3.86 emu/g (Kiatphuengporn et al. 2016). In our previous study, spinel impregnation over spherical silica with lower surface area of 178 m^2/g was found to exhibit similar ferromagnetism with magnetic value of about 7.6 emu/g (Jermy et al. 2019). Further, it has been reported that superparamagnetic effect was due to anti parallel spins of Fe^{3+} species in tetrahedral coordination site. In present study, the influence of support has shown to influence the magnetic property. The loading of spinel over mesosilicalite support tends to generate different types of nanoclusters at the pore walls (as evidenced by increased pore diameter from 3.0 to 5.9 nm). The generation of small sized nanoclusters reported to generate super paramagnetic Fe^{3+} ions, while larger nanoclusters generates ferromagnetic behavior (Cuello et al. 2017). In line with the diffuse reflectance spectra, presence of tetrahedral and octahedral species over high surface area parent mesosilicalite and MCM-41 is proposed to lead the broad hysteresis structure characteristics of ferromagnetism. The observed reduction in saturation magnetization value is mainly attributed due to presence of siloxane layers on copper spinel ferrites.

Nanostructured porous materials as drug delivery system facilitates the targeted drug delivery, reduce the in vivo dosage fluctuation, reduce drug disintegration and side effects of drugs (Ghaferi et al. 2020). In present study, a different structured nanocarriers for drug delivery was evaluated by studying the release trend of curcumin under acidic pH (pH=5.6) condition for 72 h (Fig. 4). $CuFe_2O_4$ impregnated samples were based on mesosilicalite (hexagonal micro/mesopore), SBA-16 (cubic), MCM-41 (hexagonal mesopore), Q-10 (large pore), hydrophobic silica, mesobeta (BEA large pore) and

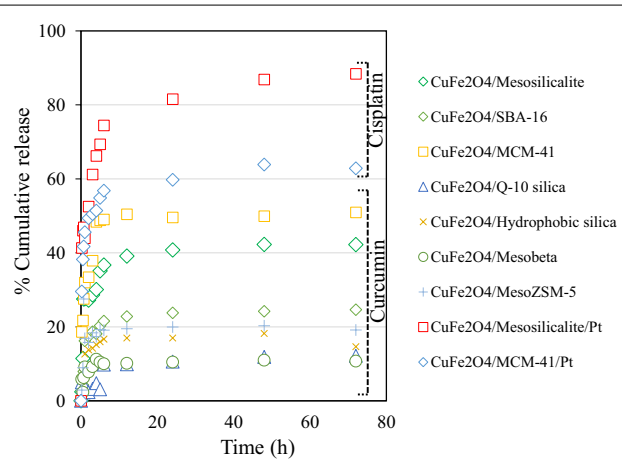

Fig. 4 Drug (curcumin, cisplatin) delivery over $CuFe_2O_4$ impregnated on different structured nanoporous materials at pH 5.6

mesoZSM-5 (MFI). The percentage cumulative release profile of curcumin over hexagonal shaped silica (MCM-41 and mesosilicalite) was found to be superior and high of about 40–50% followed by cubic shaped SBA-16. $CuFe_2O_4$/SBA-16, which contains a 3D pore architecture showed a release of about 25% for 72 h. This indicates the ink shaped pores of SBA-16 (about 3.3 nm) are slightly restricted with spinel ferrite impregnation and showed a sustained release behavior with respect to curcumin. MesoZSM-5 with MFI structure consisting of sinusoidal pores of about 0.56 nm (micropore) and spherical silica with hydrophobic character also showed a release ability at about 20%. Q-10 silica with pore size of about 18 nm and mesobeta with medium pore size of 3 nm showed comparatively a less curcumin release of 10%. The release trend shows the aluminosilicate zeolite based structured silica with medium and large pore shapes profoundly affects and induces slow release of curcumin. For quick release, hexagonal shaped channel pores of MCM-41 and mesosilicalite (micro/meso) can be utilized than cubic shaped pores of SBA-16 and aluminosilicates. Based on the present requirement, cisplatin was loaded on curcumin/$CuFe_2O_4$/mesosilicalite and curcumin/$CuFe_2O_4$/MCM-41.

In case of parent cisplatin, a quick release was reported of about 76% within 1 h. However, loading cisplatin on biodegradable polybutylcyanoacrylate polymer shown to significantly reduce such burst release and enhance both in vitro and in vivo studies (Ghaferi et al. 2020). In a similar stance, the free curcumin release was completed (100%) within 24 h. However, using solid lipid nanoparticles as nanocarriers tends to extend the drug release up to 120 h (Gupta et al. 2020). In our present study, the mesosilicalite and MCM-41 were found to promote release of cisplatin for longer duration. For instance, mesosilicalite showed about 88% of cisplatin release for 72 h, while mesopores of MCM-41 showed a release of about 63% for 72 h. This suggests that cisplatin tends to functionalize on the external micropores of mesosilicalite, while MCM-41 is able to accommodate the cisplatin inside the mesopores. The release trend of cisplatin and curcumin with the presence of both nanocarriers clearly shows the functionalization ability and advantageous of mesopores than cisplatin and curcumin alone. For different structured mesoporous nanocarrier, data analysis was done using Prism 8 software and SPSS software version 20.0 (Additional file 1: Tables S2–S5).

The Additional file 1: Table S2 shows the mean and standard deviation of curcumin drug release at pH 5. While reviewing the results, $CuFe_2O_4$/MCM-41 showed a high mean score of 40.67, whereas CuFe2O4/Q-10 Silica/Curcumin demonstrated a low mean score of 6.38. The maximum score of curcumin drug release at pH 5.6 was observed in $CuFe_2O_4$/MCM-41/Curcumin and $CuFe_2O_4$/mesoZSM-5/curcumin, however the minimum curcumin release was observed in $CuFe_2O_4$/hydrophobic silica/curcumin. From Additional file 1: Table S3, the results showed that there is significant difference between the groups with respect to curcumin release at pH 5.6 ($p < 0.05$). As significant difference was found, Scheffe's post hoc test was calculated to find out the significant difference between two groups at the same time. It is observed that the mean difference in the curcumin release between the groups such as $CuFe_2O_4$/MCM-41 and $CuFe_2O_4$/mesoZSM-5; $CuFe_2O_4$/mesosilicalite and $CuFe_2O_4$/mesoZSM-5; $CuFe_2O_4$/MCM-41 and $CuFe_2O_4$/mesoZSM-5; $CuFe_2O_4$/Q-10 silica and $CuFe_2O_4$/mesoZSM-5 was observed to be significant ($p < 0.05$). However, no significant mean difference was observed between the groups such as $CuFe_2O_4$/SBA-16 and $CuFe_2O_4$/

mesoZSM-5; $CuFe_2O_4$/Hydrophobic silica and $CuFe_2O_4$/mesoZSM-5; $CuFe_2O_4$/mesoZSM-5 and $CuFe_2O_4$/mesoZSM-5 with respect to the curcumin release ($p > 0.05$). Notably, $CuFe_2O_4$/MCM-41 showed a high mean difference score of curcumin release (40.67) with $CuFe_2O_4$/mesoZSM-5 when compared other $CuFe_2O_4$/structured silica-based nanoformulations (Additional file 1: Table S4).

Using Pearson correlation, it was inferred that $CuFe_2O_4$/MCM-41 has a significant strong and positive correlation with only $CuFe_2O_4$/Q-10 silica/curcumin ($p < 0.01$). The formulation variable $CuFe_2O_4$/mesosilicalite/curcumin showed a significant strong and positive correlation with the variables such as $CuFe_2O_4$/SBA-16/curcumin, $CuFe_2O_4$/MCM-41/curcumin, $CuFe_2O_4$/hydrophobic silica/curcumin, $CuFe_2O_4$/mesoZSM-5/curcumin, and $CuFe_2O_4$/mesobeta/curcumin ($p < 0.01$). Similarly, $CuFe_2O_4$/SBA-16/curcumin described a significant strong and positive correlation with the formulation variables such as $CuFe_2O_4$/MCM-41/curcumin, $CuFe_2O_4$/hydrophobic silica/curcumin, and CuFe2O4/mesobeta/curcumin ($p < 0.01$). Further, $CuFe_2O_4$/MCM-41/curcumin showed a significant strong and positive correlation with $CuFe_2O_4$/hydrophobic silica/curcumin and $CuFe_2O_4$/mesobeta/curcumin ($p < 0.01$). A significantly strong and positive relationship was observed between $CuFe_2O_4$/hydrophobic silica/curcumin and $CuFe_2O_4$/mesobeta/curcumin ($p < 0.01$) (Additional file 1: Table S5). On the other hand, $CuFe_2O_4$/Q-10 silica/curcumin described a significant moderate and positive correlation with $CuFe_2O_4$/mesosilicalite/curcumin, $CuFe_2O_4$/SBA-16/curcumin, and $CuFe_2O_4$/MCM-41/curcumin ($p < 0.05$). A significant moderate and positive correlation was also observed between $CuFe_2O_4$/mesoZSM-5/curcumin and $CuFe_2O_4$/hydrophobic silica/curcumin ($p < 0.05$) (Additional file 1: Table S5). To test the efficiency of our nanocomposites as potential chemotherapeutic agents, we investigated their effects on the cell viability of MCF7 (human breast cancer), HeLa (human cervical cancer), HCT116 (human colorectal. Cancer) and HFF (human foreskin fibroblast) cell lines. The cell viability assay, MTT, was performed after 48 h of treatment with the following conditions: $CuFe_2O_4$/mesosilicalite, curcumin, cisplatin, curcumin/cisplatin, $CuFe_2O_4$/mesosilicalite/curcumin, $CuFe_2O_4$/mesosilicalite/curcumin/cisplatin, and $CuFe_2O_4$/MCM-41/curcumin/cisplatin nanocomposites (Fig. 5). Treatment concentrations of $CuFe_2O_4$/mesosilicalite, $CuFe_2O_4$/mesosilicalite/curcumin, $CuFe_2O_4$/mesosilicalite/curcumin/cisplatin, and $CuFe_2O_4$/MCM-41/curcumin/cisplatin nanocomposites were: 0.025, 0.05, 0.1, and 0.5 mg/ml. While treatment concentrations for curcumin were: 0.00625, 0.0125, 0.025 and 0.125 mg/ml and that for the cisplatin group: 0.001125, 0.00225, 0.0045, and 0.0225 mg/ml. As detailed in the Materials and methods section, treatment

(See figure on next page.)

Fig. 5 Cytotoxic effects on several cancerous and control cell lines. Cell viability using MTT assay on **A** MCF7, **B** HeLa, **C** HCT116, and **B** HFF cell lines. Cells were treated with the following conditions for 48 h: $CuFe_2O_4$/mesosilicalite (group A), curcumin (group B), cisplatin (group C), curcumin/cisplatin (group D), $CuFe_2O_4$/mesosilicalite/curcumin (group E), $CuFe_2O_4$/mesosilicalite/curcumin/cisplatin (group F), and $CuFe_2O_4$/MCM-41/curcumin/cisplatin (group G). For groups A, E, F, and G treatment concentrations were as follows: 0.025, 0.05, 0.1, and 0.5 mg/ml. We used drug-loading experiments to calculate the concentration of adsorbed curcumin and cisplatin. Therefore, treatment concentrations of curcumin (group B) were: 0.00625, 0.0125, 0.025, and 0.125 mg/ml. Treatment concentrations of cisplatin (group C) were: 0.001125, 0.00225, 0.0045, 0.0225 mg/ml. n=5 independent experiments. Dashed line represents untreated cells control. Error bars ± S.E.M. Statistical analysis is shown in Additional file 1: Table S5

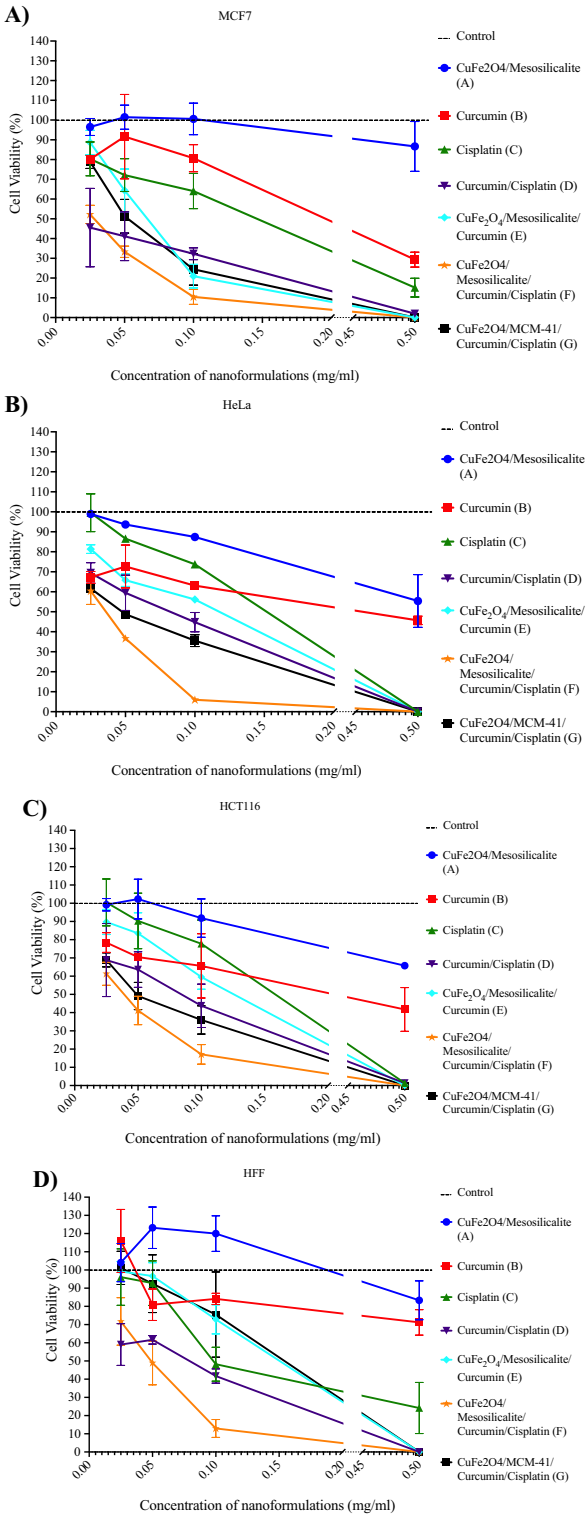

Fig. 5 (See legend on previous page.)

concentrations of curcumin and cisplatin were adjusted to reflect the actual concentration adsorbed onto the mesosilicalite nanocomposites.

Our results were analyzed by comparing data from the treated cells with the control group (untreated cells) (Additional file 1: Table S6). Cells treated with $CuFe_2O_4$/mesosilicalite nanocomposites had no effect on either MCF7, HeLa, HCT116, or HFF cells suggesting that the $CuFe_2O_4$/mesosilicalite nanocarrier did not interfere with cell viability. Pure curcumin reduced cell viability only at the highest concentration in MCF7; however, it minimally reduced the cell viability in HFF cell lines. As anticipated, pure cisplatin resulted in a reduction in cell viability in both MCF7 and HFF cell lines. Cells treated with free curcumin and cisplatin resulted in a combined effect and a greater cytotoxicity than the either one of them. Furthermore, cells that were treated with our nanocomposites $CuFe_2O_4$/mesosilicalite/curcumin, $CuFe_2O_4$/mesosilicalite/curcumin/cisplatin, and $CuFe_2O_4$/MCM-41/curcumin/cisplatin all resulted in a significant reduction in cell viability in a dose-dependent manner with $CuFe_2O_4$/MCM-41/curcumin/cisplatin having the highest effect (Fig. 5).

Upon close investigation at the third dose of treatment in MCF7 cells, the pure curcumin reduced cell viability to 80.71%, while the nanocomposites that were coated with curcumin either with or without cisplatin significantly reduced the cell viability to 20.98% (group D in Fig. 5A), and 8.96% (group E in Fig. 5A). In HeLa cells, the pure curcumin reduced cell viability to 63.07%, while the nanocomposites that were coated with curcumin without cisplatin significantly reduced the cell viability to 56.13%. In HCT116, cell viability was 65.64% and 59.5% in free curcumin and $CuFe_2O_4$/mesosilicalite/curcumin, respectively. In contrast, using the same dose on the non-cancerous cell line HFF, the pure curcumin reduced cell viability to 84.12%, whereas the nanocomposites that were coated with curcumin did not result in a significant reduction in cell viability (72.88%; group D in Fig. 5B); whereas HFF treated with nanocomposites that were coated with curcumin and functionalized with cisplatin resulted in a significant reduction in cell viability of 12.93% (group E in Fig. 5B). Interestingly, the $CuFe_2O_4$/MCM-41/curcumin/cisplatin nanocomposite (group F in Fig. 5) resulted in a significant reduction of cell viability of 24.44% in MCF7, 5.9% in HeLa, 36% in HCT116, and an insignificant reduction in viability of 75.53% in HFF. Using a drug combination of cisplatin and curcumin nanocomposites will increase the cumulative cytotoxic effects of both compounds, solve the problem of cisplatin drug resistance in tumors, and increase the bioavailability of curcumin. The $CuFe_2O_4$/mesosilicalite/curcumin/cisplatin nanocomposite had a stronger effect even at lower concentrations on all cell lines. However, using the MCM-41/mesosilicalite in our cisplatin/curcumin nanocomposite had a significant effect on MCF7, HeLa, and HCT116, while having a minimal effect on HFF. Our results suggest that using MCM-41 with our cisplatin/curcumin drug combination has the potential of affecting cancerous cells while sparing normal ones.

To calculate the EC50 of treatment conditions, we used the data from Fig. 5 to calculate the EC50 (Fig. 6). Treatment with cisplatin resulted in an EC50 of 4.425, 6.48, 6.73, and 3.763 μg/ml in MCF7, HeLa, HCT116, and HFF, respectively. Coating the $CuFe_2O_4$/mesosilicalite with curcumin resulted in an EC50 of 80.2 μg/ml in MCF7; 102.1 μg/ml in HeLa; 117.6 μg/ml in HCT116; and 141.0 μg/ml in HFF. Moreover, functionalizing the $CuFe_2O_4$/Mesosilicalite with curcumin and cisplatin resulted in an EC50 of 81.23 μg/

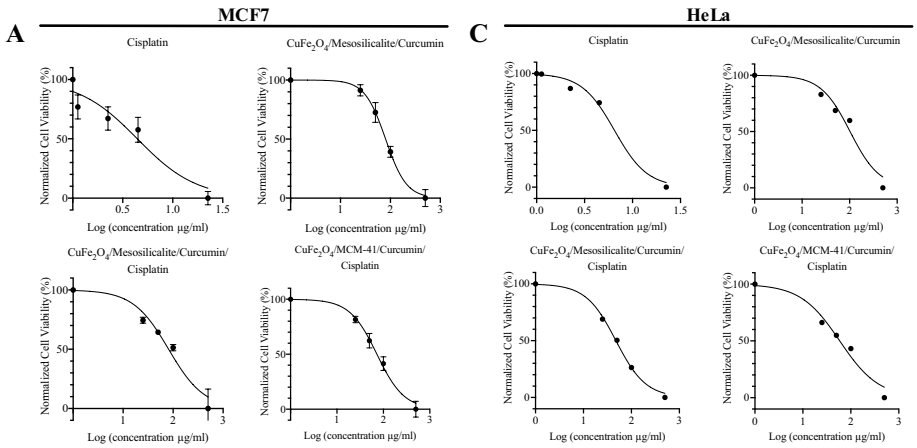

B

Drug Group	Log EC50 value	EC50 value (µg/ml)	R^2
Cisplatin	0.6459	4.425	0.7444
$CuFe_2O_4$/Mesosilicalite /Curcumin	1.904	80.20	0.9106
$CuFe_2O_4$/Mesosilicalite /Curcumin/Cisplatin	1.910	81.23	0.7990
$CuFe_2O_4$/MCM-41/ Curcumin/Cisplatin	1.860	72.51	0.9067

D

Drug Group	Log EC50 value	EC50 value (µg/ml)	R^2
Cisplatin	0.8118	6.483	0.9770
$CuFe_2O_4$/Mesosilicalite /Curcumin	2.009	102.1	0.9504
$CuFe_2O_4$/Mesosilicalite /Curcumin/Cisplatin	1.677	47.55	0.9689
$CuFe_2O_4$/MCM-41/ Curcumin/Cisplatin	1.768	58.60	0.9657

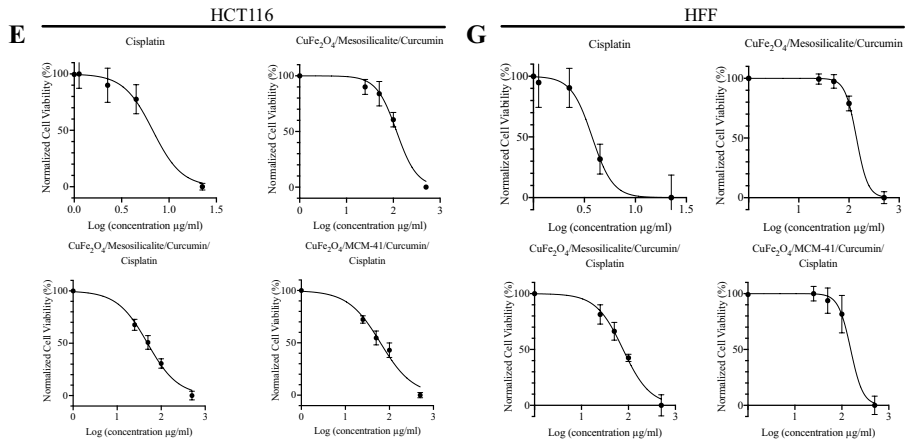

F

Drug Group	Log EC 50 value	EC 50 value (µg/ml)	R^2
Cisplatin	0.8281	6.731	0.9197
$CuFe_2O_4$/Mesosilicalite /Curcumin	2.071	117.6	0.9586
$CuFe_2O_4$/Mesosilicalite /Curcumin/Cisplatin	1.690	48.96	0.9749
$CuFe_2O_4$/MCM-41/ Curcumin/Cisplatin	1.796	62.58	0.9599

H

Drug Group	Log EC 50 value	EC 50 value (µg/ml)	R^2
Cisplatin	0.5755	3.763	0.6306
$CuFe_2O_4$/Mesosilicalite /Curcumin	2.149	141.0	0.9415
$CuFe_2O_4$/Mesosilicalite /Curcumin/Cisplatin	1.886	76.83	0.8560
$CuFe_2O_4$/MCM-41/ Curcumin/Cisplatin	2.188	154.2	0.7742

Fig. 6 EC50 analysis. Data from the cell viability assay (Fig. 5) were used to extrapolate EC50 of the following conditions: cisplatin, CuFe2O4/mesosilicalite/curcumin, CuFe2O4/mesosilicalite/curcumin/cisplatin, and CuFe2O4/MCM-41/curcumin/cisplatin. **A**, **B** Represent data from MCF7, **C**, **D** from HeLa, **E**, **F** from HCT116, and **G**, **H** from HFF cell lines. **A**, **C**, **E**, **G**) are the cell viability curves against Log concentration of each condition. **B**, **D**, **F**, **H** Represent the Log EC50, EC50, and *R*2 values of each group

ml in MCF7; 47.55 µg/ml in HeLa; 48.96 µg/ml in HCT116; and 76.83 µg/ml in HFF. However, functionalizing curcumin and cisplatin onto $CuFe_2O_4$/MCM-41 nanocomposite resulted in an EC50 of 72.51 µg/ml in MCF7; 58.6 µg/ml in HeLa; 62.58 µg/ml in HCT116; and 154.2 µg/ml in HFF. These results show that while using the mesosilicalite resulted in a similar EC50, using the MCM-41 support resulted in a 1 to 1.5

fold difference in EC50 values between HFF and the other cell lines. When comparing between our nanocomposites, our results show that both $CuFe_2O_4$/mesosilicalite/curcumin/cisplatin and $CuFe_2O_4$/MCM-41/curcumin/cisplatin nanocomposites are potential novel chemotherapeutic options. However, our results show that $CuFe_2O_4$/MCM-41/Curcumin/Cisplatin is a better candidate due to the wider difference in EC50 (a 1–1.5 fold change) between cancerous and non-cancerous cell line.

We further explored the apoptotic effects of treating cells with $CuFe_2O_4$/mesosilicalite/curcumin, $CuFe_2O_4$/mesosilicalite/curcumin/cisplatin, and $CuFe_2O_4$/MCM-41/curcumin/cisplatin nanocomposites. Cells were viewed under light and fluorescent microscopes (Fig. 7). For the latter, cells were stained with the apoptotic marker cleaved-Caspase 3 (c-Caspase 3), and Hoechst, which is a nuclear marker. Our images clearly showed cells stained with c-Caspase 3 (magenta), which is the activated form of the protein, after treatment with our nanocomposites for 48 h. These results suggest that our nanocomposites significantly reduce cell viability by activating apoptosis.

Here, we explored merging two compounds that have potential benefits, but suffer from several side effects: curcumin and cisplatin. Curcumin has been extensively investigated as a chemotherapeutic agent in breast cancer, hepatocellular carcinoma, pancreatic cancer, gastric cancer, osteoclastoma, and bladder cancer (Syng-Ai et al. 2004; Zhu and Bu 2017; Li et al. 2017; Cao et al. 2015; Zhang et al. 2018). It has been found to activate JNK pathway, induce the generation of reactive oxygen species (ROS), and subsequently apoptosis (Syng-Ai et al. 2004; Zhu and Bu 2017). However, curcumin has some problems that hinder its full potential such as low solubility, low bioavailability, and rapid

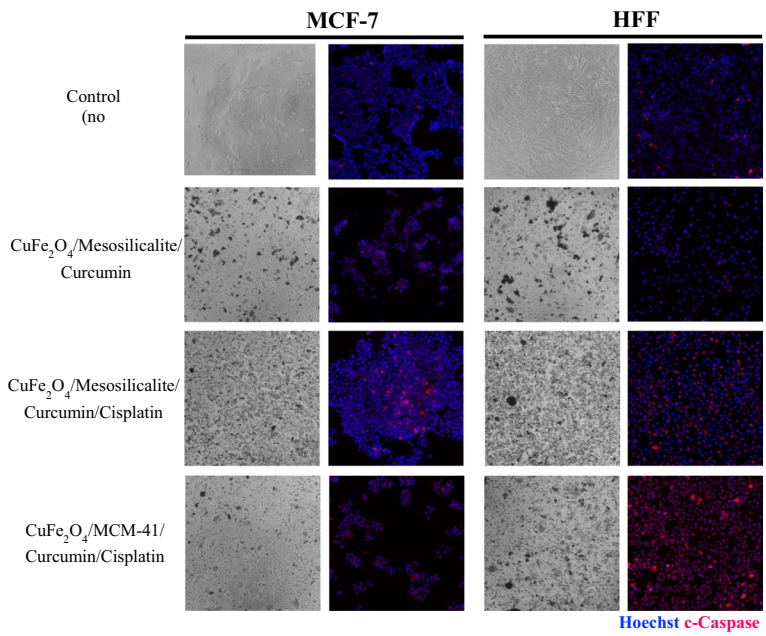

Fig. 7 Apoptotic effect of different treatment conditions on MCF7 and HFF. Cells were treated with: $CuFe_2O_4$/mesosilicalite/curcumin, $CuFe_2O_4$/mesosilicalite/curcumin/cisplatin, and $CuFe_2O_4$/MCM-41/curcumin/cisplatin at a concentration of 0.5 mg/ml for 48 h. Left column is light microscopy images, while right column is fluorescence microscopy images (not taken from the same field). For the immunofluorescence images, cells were stained with cleaved-Caspase 3 (magenta) and Hoechst (blue)

elimination from the body (Anand et al. 2007). Research is being conducted to increase the bioavailability of curcumin. On the other hand, cisplatin is a well-established chemotherapeutic drug. Unfortunately, it is fraught with several issues such as drug resistance and systemic toxicity (Dasari and Tchounwou 2014). The mechanism of action of cisplatin is by activating the JNK pathway and inducing oxidative stress, DNA damage, and apoptosis. However, cisplatin will also result in increased levels of Glutathione S transferase (GST), resulting in a reduction in ROS, and resistance to cisplatin. Therefore, a combination treatment of cisplatin and curcumin, which increases ROS, might augment the cytotoxic effect and prevent cisplatin-related drug resistance (Townsend and Tew 2003).Curcumin was shown to have a synergistic effect with cisplatin and enhance the cytotoxic effect in non-small cell lung cancer and laryngeal squamous cancer cell lines (Abdul Satar et al. 2021; Gökçe Kütük et al. 2019). A combinational drug mixtures of curcumin (B) and cisplatin (C) with varying concentrations (20.7025 μM, 41.405 μM, 82.8099 μM, 414.0495 μM) of were taken and studied on different cell lines such as MCF-7, HeLa, HCT116 cancer cells and HFF normal cells (Additional file 1: Table S5 and Fig. 5A–D). Combinational drug without nanocarrier decreases the cell viability of the MCF-7, He La, HCT116 cells and also HFF normal cells. Curcumin and cisplatin combinational drug clearly show a synergistic effect. Cisplatin has toxicity on normal cells. On the other hand, loading of combinational drugs on nanocomposite also showed cytotoxicity effects on cancer cells except HFF cells. The results show that the prepared nanoformulation containing curcumin with cisplatin reduce the toxicity in normal cells. Potential therapeutic approach of using curcumin may enhance the effects of cisplatin by targeting the cancer cells. The presence of high surface area $CuFe_2O_4$/MCM-41 nanocarrier helps to synergistic action of dual drugs and maintaining a sustained release of drugs could assist selectively targeting cancer cells.

In addition, loading of such dual combinational drugs on a biodegradable polymer based on polycaprolactone, linked with Pt using amine based polymer and PEG shell exhibited a synergistic effect (combination index = 0.4–0.8) with dual delivery in one nanocarrier against multidrug resistant cancer. The use of polymeric nanocarrier improves the transport of curcumin and cisplatin in to the cells by endocytosis (Scarano et al. 2015). Our results show that a simple coating of curcumin and functionalization of cisplatin into hexagonal pore structural framework of silica had a significant effect on the cytotoxic effectiveness of nanocomposites on various cancer cells.

We previously tested cisplatin-functionalized cubic spinel $CuFe_2O_4$ loaded on monodispersed spherical hydrophilic silica (HYPS) nanoparticles on MCF7 breast cancer cells (Jermy et al. 2019). In our current work, we investigated two nanoformulations using the hexagonally shaped silica: (a) the mesosilicalite with zeolite (strong) framework, and (b) the MCM-41 with amorphous (weak) framework. Both of which were coated with curcumin and functionalized with cisplatin. While the EC50 of our previous spherical shaped silica nanoformulation was equal to 180.89 μg/ml (Jermy et al. 2019), our current hexagonal shaped silica nanocomposites were 81.23 μg/ml (mesosilicalite) and 72.51 μg/ml (MCM-41).

The present study clearly indicates that changing the structural framework from spherical to hexagonally shaped silica increased the chemotherapeutic efficiency and reduced the EC50 values. The improved effectiveness is most likely attributed to the

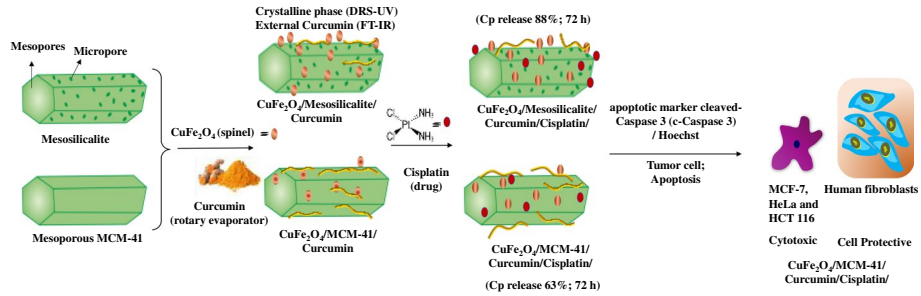

Scheme 1: Spinel ferrite/mesosilicalite and MCM-41 nanocomposite for curcumin–cisplatin bound nanotherapeutic effect against MCF-7, HeLa and HCT 116 cancer cell lines

increased loading capacity in the hexagonally shaped nanocomposites as indicated in the drug release studies (Fig. 4).

$CuFe_2O_4$/mesosilicalite/curcumin/cisplatin, and $CuFe_2O_4$/MCM-41/curcumin/cisplatin nanocomposites utilize the benefits of curcumin and cisplatin. This combination resulted in novel nanocomposites that significantly reduced cell viability of the MCF7 breast cancer cell line by activating the apoptotic pathway as indicated by c-caspase 3. Our results show that both $CuFe_2O_4$/mesosilicalite/curcumin/cisplatin and $CuFe_2O_4$/MCM-41/curcumin/cisplatin nanocomposites are potential novel chemotherapeutic options. However, $CuFe_2O_4$/MCM-41/curcumin/cisplatin nanocomposites offer an added advantage of a wider gap in cytotoxicity between cancerous and non-cancerous cell lines (Scheme 1).

Conclusions

Synergistic action of curcumin and cisplatin on structured magnetically active hexagonal nanocarriers was studied for targeted combinational therapeutics. Mesoporous MCM-41 and mesosilicalite with micro/mesopores were developed and impregnated with copper spinel ferrite. The textural characteristics have been analyzed with various physico-chemical techniques. A significant difference in curcumin release was observed among the different $CuFe_2O_4$/structured silica-based nanoformulations. Also, those $CuFe_2O_4$/MCM-41 structured silica-based nanoformulations showed a significant positive relationship with each other. $CuFe_2O_4$/mesosilicalite followed by $CuFe_2O_4$/MCM-41 with high curcumin release ability was further functionalized with cisplatin. The effects of our nanocomposite on cell viability of MCF7 and HFF cell lines were tested. Treatment with either $CuFe_2O_4$/mesosilicalite/curcumin/cisplatin or $CuFe_2O_4$/MCM-41/curcumin/cisplatin nanocomposites resulted in a significant reduction in cell viability that was greater than treatment with either curcumin or cisplatin. Furthermore, cells treated with our two nanocomposites had a higher number of c-Caspase 3-positive cells than the untreated control. These results suggest that the reduction in cell viability is triggered by activating the apoptotic signaling pathway. The EC50 for $CuFe_2O_4$/mesosilicalite/curcumin/cisplatin was 81.23 μg/ml in MCF7; 47.55 μg/ml in HeLa; 48.96 μg/ml in HCT116 and 76.83 μg/ml in HFF. The EC50 for $CuFe_2O_4$/MCM-41/curcumin/cisplatin was 72.51 μg/ml in MCF7; 58.6 μg/ml in HeLa; 62.58 μg/ml in HCT116; and 154.2 μg/ml in HFF. Our results show that both nanocomposites can be further explored

as potential novel chemotherapeutic options. $CuFe_2O_4$/MCM-41/curcumin/cisplatin nanocomposites offer the added advantage of a wider gap in cytotoxicity between cancerous and non-cancerous cell lines.

Supplementary Information

The online version contains supplementary material available at https://doi.org/10.1186/s12645-021-00106-7.

Additional file 1: Figure S1. X-ray diffraction pattern of $CuFe_2O_4$ impregnated on different structured mesoporous materials. **Figure S2.** Nitrogen adsorption-desorption isotherm of $CuFe_2O_4$ impregnated on different structured mesoporous materials (**a**) $CuFe_2O_4$/Q-10 silica, (**b**) $CuFe_2O_4$/SBA-16, (**c**) $CuFe_2O_4$/Hydrophobic silica, (**d**) $CuFe_2O_4$/MesoZSM-5, (**e**) $CuFe_2O_4$/Mesobeta. **Figure S3.** Pore size distributions of $CuFe_2O_4$ impregnated on different structured mesoporous materials (**a**) $CuFe_2O_4$/Q-10 silica, (**b**) $CuFe_2O_4$/SBA-16, (**c**) $CuFe_2O_4$/Hydrophobic silica, (**d**) $CuFe_2O_4$/MesoZSM-5, (**e**) $CuFe_2O_4$/Mesobeta. **Figure S4.** Vibrating sample magnetometer analysis of (**a**) $CuFe_2O_4$/MCM-41 and (**b**) $CuFe_2O_4$/Mesosilicalite. **Table S1.** Textural characteristics of 30% $CuFe_2O_4$ impregnated on different mesostructured materials. **Table S2.** Descriptive statistics of curcumin release over different $CuFe_2O_4$/structured silica based nanoformulations. **Table S3.** Curcumin release over different $CuFe_2O_4$/structured silica based nanoformulations (One way ANOVA). **Table S4.** Post hoc tests for mean difference in curcumin release among different $CuFe_2O_4$/structured silica based nanoformulations. **Table S5.** Pearson correlation of curcumin release over different $CuFe_2O_4$/structured silica based nanoformulations. **Table S6.** Statistical analysis of the cell viability assay performed on (**A**) MCF7, (**B**) HeLa, (**C**) HCT116, and (**D**) HFF cell lines. Analysis of drug treated was performed compared to cell control (without treatment) using 2way ANOVA with Dunnett's post hoc test. $*p < 0.05$; $**p < 0.01$; $***p < 0.001$; $****p < 0.0001$; *ns* not significant.

Acknowledgements
Rabindran Jermy would like to acknowledge the advanced state of art facilities provided by Institute for Research and Medical Consultations (IRMC), Imam Abdulrahman Bin Faisal University, Dammam, Saudi Arabia. The authors would like to acknowledge Ms. Dorothy Joy H. Huelar for her assistance in the in vitro studies. Technical assistance of Ms. Janaica Yu Logan is acknowledged.

Authors' contributions
Conception and design: BRJ, VR. Data acquisition: BRJ, DA. Investigation, analysis and interpretation: DA, WAA, VR. Software, microscope and validation: RMP, HD, investigation: NA, AAA, TMA. Drafting article: VR, DA, BRJ. Final approval of article: BRJ, VR. All authors read and approved the final manuscript.

Funding
Rabindran Jermy would like to acknowledge the funding from Deanship of Scientific Research (DSR), Imam Abdulrahman Bin Faisal University with grant number 2018-025-IRMC.

Availability of data and materials
The data obtained in this study are provided in this manuscript and in supplementary file. Further additional data can be provided by corresponding authors upon request.

Declarations

Ethics approval and consent to participate
Not applicable.

Consent for publication
Not applicable.

Competing interests
The authors declare that they have no competing interests.

Author details
[1]Department of Nano-Medicine Research, Institute for Research and Medical Consultations, Imam Abdulrahman Bin Faisal University, P.O. Box 1982, Dammam 31441, Saudi Arabia. [2]Department of Stem Cell Research, Institute for Research and Medical Consultations, Imam Abdulrahman Bin Faisal University, P.O. Box 1982, Dammam 3144, Saudi Arabia. [3]Department of Neuroscience Research, Institute for Research and Medical Consultations, Imam Abdulrahman Bin Faisal University, P.O. Box 1982, Dammam 31441, Saudi Arabia. [4]Deanship of Quality and Academic Accreditation, Imam Abdulrahman Bin Faisal University, Post Box No. 1982, Dammam 31441, Saudi Arabia. [5]Cell and Molecular Biology, Department of Biology, College of Science, Imam Abdulrahman Bin Faisal University, P.O. Box 1982, Dammam 31441, Saudi Arabia. [6]College of Engineering Research (CER), King Fahd University of Petroleum and Minerals, Dhahran 31261, Saudi Arabia. [7]Deanship of Scientific Research & Department of Nano-Medicine Research, Institute for Research and Medical Consultations, Imam Abdulrahman Bin Faisal University, P.O. Box 1982, Dammam 31441, Saudi Arabia.

Received: 13 August 2021 Accepted: 9 November 2021
Published online: 27 November 2021

References

Abdul Satar N, Ismail MN, Yahaya BH (2021) Synergistic roles of curcumin in sensitising the cisplatin effect on a cancer stem cell-like population derived from non-small cell lung cancer cell lines. Molecules 26:1056. https://doi.org/10.3390/molecules26041056

Abduljauwad SN, Ahmed HU (2019) Enhancing cancer cell adhesion with clay nanoparticles for countering metastasis. Sci Rep 9(1):5935. https://doi.org/10.1038/s41598-019-42498-y

Akbarzadeh I, Yaraki MT, Ahmadi S, Chiani M, Nourouzian D (2020) Folic acid-functionalized niosomal nanoparticles for selective dual-drug delivery into breast cancer cells: an in-vitro investigation. Adv Powder Technol 31:4064–4071. https://doi.org/10.1016/j.apt.2020.08.011

Amiri M, Salavati-Niasari M, Akbari A (2019) Magnetic nanocarriers: evolution of spinel ferrites for medical applications. Adv Coll Interface Sci 265:29–44

Anand P, Kunnumakkara AB, Newman RA, Aggarwalm BB (2007) Bioavailability of curcumin: problems and promises. Mol Pharm 4:807–818. https://doi.org/10.1021/mp700113r (**Epub 2007 Nov 14 PMID: 17999464**)

Beck JS, Vartuli JC, Roth WJ, Leonowicz ME, Kresge CT, Schmitt KD, Chu CT, Olson DH, Sheppard EW, McCullen SB, Higgins JB (1992) A new family of mesoporous molecular sieves prepared with liquid crystal templates. J Am Chem Soc 14(27):10834–10843. https://doi.org/10.1021/ja00053a020

Bhandari R, Gupta P, Dziubla T, Hilt JZ (2016) Single step synthesis, characterization and applications of curcumin functionalized iron oxide magnetic nanoparticles. Mater Sci Eng C Mater Biol Appl 67:59–64. https://doi.org/10.1016/j.msec.2016.04.093

Cao F, Liu T, Xu Y, Xu D, Feng S (2015) Curcumin inhibits cell proliferation and promotes apoptosis in human osteoclastoma cell through MMP-9, NF-κB and JNK signaling pathways. Int J Clin Exp Pathol 8:6037–6045

Chen Y, Lu Y, Lee RJ, Xiang G (2020) Nano Encapsulated Curcumin: And Its Potential for Biomedical Applications. Int J Nanomed 15:3099–3120. https://doi.org/10.2147/IJN.S210320

Cuello NI, Elías VR, Mendieta SN, Longhi M, Crivello ME, Oliva MI, Eimer GA (2017) Drug release profiles of modified MCM-41 with superparamagnetic behavior correlated with the employed synthesis method. Mater Sci Eng C Mater Biol Appl 78:674–681. https://doi.org/10.1016/j.msec.2017.02.010.N.I

Dasari S, Tchounwou PB (2014) Cisplatin in cancer therapy: molecular mechanisms of action. European J Pharmacol 740:364–378. https://doi.org/10.1016/j.ejphar.2014.07.025

de Lima HHC, Kupfer VL, Moisés MP, Guilherme MR, de C Rinaldi J, Felisbino SL, Rubira AF, Rinaldi AW, (2018) Bionanocomposites based on mesoporous silica and alginate for enhanced drug delivery. Carbohydr Polym 196:126–134. https://doi.org/10.1016/j.carbpol.2018.04.107

Dippong T, Levei EA, Cadar O (2021) Recent advances in synthesis and applications of MFe2O4 (M = Co, Cu, Mn, Ni, Zn) nanoparticles. Nanomaterials 11:1560. https://doi.org/10.3390/nano11061560

Ghaferi M, Amari S, Vivek Mohrir B, Raza A, Ebrahimi Shahmabadi H, Alavi SE (2020) Preparation, characterization, and evaluation of cisplatin-loaded polybutylcyanoacrylate nanoparticles with improved in vitro and in vivo anticancer activities. Pharmaceuticals 13(3):44. https://doi.org/10.3390/ph13030044

Ghosh AK, Samanta I, Mondal A, Liu WR (2019) Covalent Inhibition in drug discovery. ChemMedChem 14:889–906

Gökçe Kütük S, Gökçe G, Kütük M, Gürses Cila HE, Nazıroğlu M (2019) Curcumin enhances cisplatin-induced human laryngeal squamous cancer cell death through activation of TRPM2 channel and mitochondrial oxidative stress. Sci Rep 9:17784. https://doi.org/10.1038/s41598-019-54284-x

Gupta T, Singh J, Kaur S, Sandhu S, Singh G, Kaur IP (2020) Enhancing bioavailability and stability of curcumin using solid lipid nanoparticles (CLEN): a covenant for its effectiveness. Front Bioeng Biotechnol 8:879. https://doi.org/10.3389/fbioe.2020.00879

Jermy BR, Ravinayagam V (2019) Hierarchical ZSM-5 based MCM-41 aluminosilicates: Ostwald ripening effect of 8 years old aged samples. Adv Nat Sci 10(4):045003. https://doi.org/10.1088/2043-6254/ab4876

Jermy BR, Ravinayagam V, Alamoudi WA, Almohazey D, Dafalla H, Hussain Allehaibi L, Baykal A, Toprak MS, Somanathan T (2019) Targeted therapeutic effect against the breast cancer cell line MCF-7 with a CuFe2O4/silica/cisplatin nanocomposite formulation. Beilstein J Nanotechnol 10:2217–2228. https://doi.org/10.3762/bjnano.10.214

Karthikeyan A, Senthil N, Min T (2020) Nanocurcumin: a promising candidate for therapeutic applications. Front Pharmacol 11:487. https://doi.org/10.3389/fphar.2020.00487

Kefeni KK, Mamba BB (2020) Photocatalytic application of spinel ferrite nanoparticles and nanocomposites in wastewater treatment: review. Sustain Mater Technol 23:e00140

Khanna L, Gupta G, Tripathi SK (2019) Effect of size and silica coating on structural, magnetic as well as cytotoxicity properties of copper ferrite nanoparticles. Mater Sci Eng C 97:552–566

Kiatphuengporn S, Jantaratana P, Limtrakul J, Chareonpanich M (2016) Magnetic field-enhanced catalytic CO2 hydrogenation and selective conversion to light hydrocarbons over Fe/MCM-41 catalysts. Chem Eng J 306:866–875. https://doi.org/10.1016/j.cej.2016.08.029

Lanzafame P, Papanikolaou G, Perathoner S, Centi G, Giordano G, Migliori M (2020) Weakly acidic zeolites: a review on uses and relationship between nature of the active sites and catalytic behaviour. Microp Mesop Mater 300:110157. https://doi.org/10.1016/j.micromeso.2020.110157

Li X, Gao Y (2020) Synergistically fabricated polymeric nanoparticles featuring dual drug delivery system to enhance the nursing care of cervical cancer. Process Biochem 98:254–261. https://doi.org/10.1016/j.procbio.2020.09.010

Li W, Zhou Y, Yang J, Li H, Zhang H, Zheng P (2017) Curcumin induces apoptotic cell death and protective autophagy in human gastric cancer cells. Oncol Rep 37:3459–3466. https://doi.org/10.3892/or.2017.5637

Li C, Wang J, Wang Y, Gao H, Wei G, Huang Y, Yu H, Gan Y, Wang Y, Mei L, Chen H, Hu H, Zhang Z, Jin Y (2019) Recent progress in drug delivery. Acta Pharm Sin b 9(6):1145–1162. https://doi.org/10.1016/j.apsb.2019.08.003

Mantha S, Pillai S, Khayambashi P, Upadhyay A, Zhang Y, Tao O, Pham HM, Tran SD (2019) Smart hydrogels in tissue engineering and regenerative medicine. Materials (basel) 12(20):3323. https://doi.org/10.3390/ma12203323

Mohan PK, Sreelakshmi G, Muraleedharan CV, Joseph R (2012) Water soluble complexes of curcumin with cyclodextrins: Characterization by FT-Raman spectroscopy. Vib Spectrosc 62:77–84. https://doi.org/10.1016/j.vibspec.2012.05.002

Mosmann T (1983) Rapid colorimetric assay for cellular growth and survival: application to proliferation and cytotoxicity assays. J Immunol Methods 65:55–63. https://doi.org/10.1016/0022-1759(83)90303-4
Najmoddin N, Beitollahi A, Devlin E, Kavas H, Mohseni SM, Åkerman J, Niarchos D, Rezaie H, Muhammed M, Toprak MS (2014) Magnetic properties of crystalline mesoporous Zn-substituted copper ferrite synthesized under nanoconfinement in silica matrix. Microporous Mesoporous Mater 190:346–355. https://doi.org/10.1016/j.micromeso.2014.02.033
Odedairo T, Balasamy RJ, Al-Khattaf S (2012) Aromatic transformations over aluminosilicate micro/mesoporous composite materials. Catal Sci Technol 2(6):1275–1286. https://doi.org/10.1039/C2CY00547F
Ravinayagam V, Jermy BR (2017) Studying the loading effect of acidic type antioxidant on amorphous silica nanoparticle carriers. J Nanopart Res 19(6):1–4. https://doi.org/10.1007/s11051-017-3874-y
Ravinayagam V, Jermy BR (2019) Fabricating hierarchical ZSM-5 to induct long chain antioxidant coenzyme Q10 for biomedical application. J Saudi Chem Soc 23(4):461–476. https://doi.org/10.1016/j.jscs.2018.09.001
Sauraj VK, Kumar B, Priyadarshi R, Deeba F, Kulshreshtha A, Kumar A, Agrawal G, Gopinath P, Negi YS (2020) Redox responsive xylan-SS-curcumin prodrug nanoparticles for dual drug delivery in cancer therapy. Mater Sci Eng C Mater Biol Appl 107:110356. https://doi.org/10.1016/j.msec.2019.110356
Scarano W, de Souza P, Stenzel MH (2015) Dual-drug delivery of curcumin and platinum drugs in polymeric micelles enhances the synergistic effects: a double act for the treatment of multidrug-resistant cancer. Biomater Sci 3(1):163–174. https://doi.org/10.1039/c4bm00272e
Syng-Ai C, Kumari AL, Khar A (2004) Effect of curcumin on normal and tumor cells: role of glutathione and bcl-2. Mol Cancer Ther 3(9):1101–1108 (**PMID: 15367704**)
Townsend DM, Tew KD (2003) The role of glutathione- S -transferase in anti-cancer drug resistance. Oncogene 22:7369–7375. https://doi.org/10.1038/sj.onc.1206940
Wang F, Li J, Tang X, Huang K, Chen L (2020) Polyelectrolyte three layer nanoparticles of chitosan/dextran sulfate/chitosan for dual drug delivery. Colloids Surf, B 190:110925. https://doi.org/10.1016/j.colsurfb.2020.110925
Zhang L, Yang G, Zhang R, Dong L, Chen H, Bo J, Xue W, Huang Y (2018) Curcumin inhibits cell proliferation and motility via suppression of TROP2 in bladder cancer cells. Int J Oncol 53:515–526. https://doi.org/10.3892/ijo.2018.4423
Zhu Y, Bu S (2017) Curcumin induces autophagy, apoptosis, and cell cycle arrest in human pancreatic cancer cells. Evid Based Complem Altern Med. https://doi.org/10.1155/2017/5787218

Publisher's Note